J. Fluid Mech. (1992), *vol.* 242, *pp.* 145–168
Printed in Great Britain

The standing hydraulic jump: theory, computations and comparisons with experiments

By R. I. BOWLES AND F. T. SMITH
Department of Mathematics, University College London, Gower Street, London WC1E 6BT, UK

(Received 19 February 1991 and in revised form 9 February 1992)

In this theoretical and computational study of the flow of a liquid layer, under the influence of surface tension and gravity most notably, the nonlinear equations governing an interaction between viscous effects and the effects of surface tension, gravity and streamline curvature for the limit of large Reynolds numbers are derived. The aim is to make a comparison between the predictions of this theory and the experiments of Craik *et al.* on the axisymmetric hydraulic jump. Such a jump is commonly encountered in the everyday context of the initial filling of a kitchen sink, for example, and it is found in the present work that initially all the effects listed above can play a primary role in practice in the local jump phenomenon. As a first step here, the flow of the layer over a small obstacle is considered. It is seen that as surface tension becomes increasingly significant the upstream influence becomes more wave-like. Second, calculations and analysis of the nonlinear free interaction are presented and show wave-like behaviour upstream, followed downstream by a depth profile not unlike that in the typical hydraulic jump. The effects of gravity dominate those of surface tension downstream. Finally, comparisons are made with the experiments and show fair quantitative agreement, supporting the present proposition that these hydraulic jumps are caused by boundary-layer separation due to a viscous–inviscid interaction forced by downstream boundary conditions on, in this case, a fully developed, high-Froude-number liquid layer.

1. Introduction

Experiments performed by Craik *et al.* (1981) study the axisymmetric hydraulic jump formed when a column of liquid falls vertically onto a flat surface and spreads horizontally, just as from a tap into a kitchen sink. Similar experiments have been performed by Larras (1962), Clarke (1970) and Watson (1964). In this paper we make a comparison between the experiments of Craik *et al.* and the present theory which is based on the proposal that the jump is, at its start, a relatively abrupt phenomenon described by a nonlinear interaction between the effects of viscosity and the inviscid mechanisms of surface tension, cross-stream pressure gradients induced by streamline curvature, and gravity. This interaction is the source of a non-uniqueness or upstream influence in the solution of the governing equations and the jump itself is the final form of a free interaction solution which branches from the upstream undisturbed flow solution, adjusting the flow in readiness for downstream conditions. We presume this flow to be laminar and fully developed and that the Froude number of the flow is large, in line with the typical experimental conditions above and with those holding in the everyday context of the kitchen sink flow.

The interpretation of a hydraulic jump as the result of a viscous–inviscid

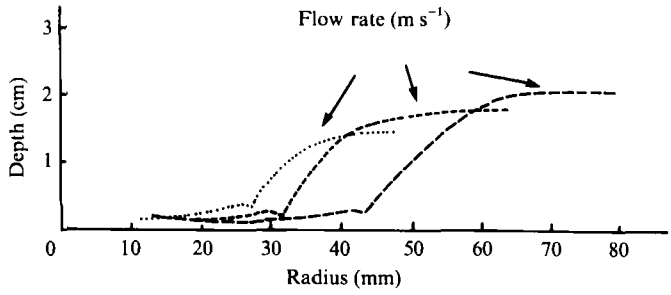

FIGURE 1. The experimental results of Craik *et al.* (1981) for hydraulic jumps.

interaction is not a new idea. Gajjar & Smith (1983) consider the surface-tension-free flow of a liquid layer with a uniform velocity profile, allied to a viscous sublayer at the wall to ensure that the no-slip condition is met. They show that for an order-one Froude number in the limit of large Reynolds number (Re), branching or free interaction can take place on a lengthscale L, where $1 \ll L \ll Re$ if the Froude number is greater than one. The normalized governing equations are shown to be identical with those which govern the hypersonic free interaction, with the displacement of the viscous sublayer ($-A$) and the pressure (P) driving that layer being proportional, or in scaled terms $P = -A$. In the context of liquid-layer flow the displacement, $-A$, is identified with the change in height of the free surface and so the driving pressure gradient is just that provided by the effects of gravity. The lengthscale of these interactions is sufficiently long that streamline curvature effects are relatively small and sufficiently short that viscous effects are confined to a sublayer at the wall. Having established that the uniform flow is not a unique solution to the governing equations over these scales Gajjar & Smith go on to examine the far-downstream asymptote of the interaction and show that free-surface height increases like $P_1 \bar{x}^m$ ($P_1 = 0.947\,96$), where $\bar{x}$ is the scaled streamwise distance and $m = \frac{2}{3}(\sqrt{7}-2) \approx 0.430\,50$. Thus the free surface there has a blunt shape, approximately parabolic and qualitatively not unlike the real hydraulic jump.

Brotherton-Ratcliffe & Smith (1986) make a comparison of the theory of Gajjar & Smith with the experiments of Craik *et al.* They presume that the flow properties upstream of the jump are essentially inviscid, but with a Blasius sublayer at the wall. This is used to give predictions for the depth and skin friction of the flow at the radius of the jump. It implies that the depth varies inversely as the radius, due to mass continuity effects, and that the skin friction varies as the inverse square root of the radius, due to the growing boundary layer. Overall, however, the prediction for the height of the jump is too small. The comparison is most accurate in the case where the incident depth used in the prediction is not that calculated as above but that measured from figure 6 of Craik *et al.*, reproduced here as figure 1. In fact the inviscid theory predicts the upstream depth to be approximately a fifth of its actual value. On the other hand, there are many encouraging features of qualitative agreement between the behaviour and structure of the experimental jumps and the predictions of the high-Reynolds-number interactive theory. For example, in the experiments the main body of the layer does not slow suddenly, but instead seems to ride over a separated region below it, of length large compared with the depth of the layer. This is in contrast to the assumptions of traditional inviscid models of the hydraulic jump (Rayleigh 1914; Lamb 1932; Watson 1964; Lighthill 1978) which model the jump as a discontinuity in the flow field. The theoretical prediction here is that the flow should react in two regions with separation possible in the viscous sublayer but the

main part of the flow merely being displaced. In addition, in the experiments, as the position of the jump moves (quasi-steadily according to the present theory) towards the source of the water the length of the separated region decreases. This can be explained as being due to an increase in the skin friction or the Froude number in the thinner, faster-moving layer nearer the source, implying, from the scalings involved (which are presented below), a decrease in the lengthscale of the interaction.

Despite the relative success of the above theory and comparison, we believe that significant additional effects should be included in the theory. An examination of figure 1 suggests two main effects which are not considered above. The first of these is the effect of viscosity in the incident profile upstream of the jump. It is this that is responsible for the substantial increase in thickness of the incident layer ahead of the free interaction rather than the decrease predicted by inviscid theory. Watson's (1964) solution, which takes account of viscous effects in the upstream profile, predicts a quadratic increase in the depth of the layer, as viscous retardation more than compensates for the effects of radial spreading. The second main effect is that of surface tension – in the experiments and in the filling of a kitchen sink one or more small standing waves can be seen upstream of the predominant jump. Although it is tempting to interpret these as capillary waves, the present theory shows that, rather, they are inherent features of the overall viscous–inviscid interaction described below. There is also a third effect which we include in the theory below, that of the cross-stream pressure gradient due to streamline curvature. This is included since it acts to reduce the effect of the surface tension, giving rise to a term in the pressure-displacement law of the same type as does surface tension but of a different sign. Although the emphasis of this work is on the study of the steady hydraulic jump, many of the experiments of Craik *et al.* and others indicate unsteady jumps, exhibiting waves, instability and transition to turbulent flow. The theory presented here can be extended to unsteady flow, and indeed the unsteady version of the governing equations seems to merit further study, for example in view of the nonlinear breakup within finite time predicted by Smith (1988).

We therefore develop a theory of the hydraulic jump along these lines, on the assumption that the Reynolds number of the flow is large but also that the Froude number is large, sufficiently large, in fact, that Watson's solution is an adequate description of the layer upstream of the jump. This assumption also ensures that the branching solutions initially arise on an essentially parallel basic flow. We consider first the flow of a two-dimensional layer (in §2) and derive the equations governing the interaction on a long $O(Re)$ scale over which curvature effects are small. In the limit of large Froude number, however, the scale of the interaction decreases and when the Froude number is $O(Re^{\frac{2}{7}})$ the curvature effects cannot be neglected and new equations incorporating them are derived. We then consider (in §3) the solution of a linearized form of these equations corresponding to the flow of the layer over an obstacle of small height relative to the depth of the inner layer. This illustrates the change in nature of the upstream solution from smooth to wave-like as the effects of surface tension become increasingly important. Following that, we describe numerical solutions to the nonlinear free interaction and analytical properties in §4. Finally we incorporate these results into a theory of the axisymmetric jump encountered in the experiments, and compare the two in §5, followed by further discussion in §6. The comparison is found to yield fairly good agreement in quantitative terms. This comparison appears to give the simplest experimental verification (so far at least) of viscous–inviscid interaction theory, in the sense that the hydraulic jump is an everyday occurrence.

2. The equations governing a two-dimensional jump

2.1. *Long scales*

The physical set-up of the problem is illustrated in figure 2. We consider two-dimensional motions. Let $X^* = 0$ be the station at which we are considering the flow, and let the depth and velocity profile here be h^* and $U^*(y^*/h^*)$ respectively. Here y^* is the vertical coordinate. The volume flux per unit width, Q^*, carried in the layer, is independent of X^*, and if the kinematic viscosity of the fluid is ν we can define a Reynolds number for the flow as Q^*/ν. A typical velocity at the particular X^*-station is $\tilde{U}^* = Q^*/h^*$ and a representative pressure is $\rho g h^*$, where ρ is the fluid density. We take h^* as a typical lengthscale. If we non-dimensionalize the Navier–Stokes equations with respect to these values we find

$$\bar{U}\bar{U}_{\hat{X}} + \hat{V}\bar{U}_y = -s\bar{P}_{\hat{X}} + Re^{-1}(\bar{U}_{yy} + \bar{U}_{\hat{X}\hat{X}}), \tag{2.1a}$$

$$\bar{U}\hat{V}_{\hat{X}} + \hat{V}\hat{V}_y = -s\bar{P}_y - s + Re^{-1}(\hat{V}_{yy} + \hat{V}_{\hat{X}\hat{X}}), \tag{2.1b}$$

$$\bar{U}_{\hat{X}} + \hat{V}_y = 0, \tag{2.1c}$$

$$\bar{U} = \hat{V} = 0 \quad \text{at} \quad y = 0, \tag{2.1d}$$

$$\int_0^{1+\eta(\hat{X})} \bar{U}(y)\,dy = 1. \tag{2.1e}$$

Here $y = 1+\eta(\hat{X}) \equiv h(\hat{X})$ is the unknown position of the free surface. We define s to be the inverse Froude number of the problem, $s = Fr^{-1} = gh^{*3}/Q^{*2}$, where g is the acceleration due to gravity. If we neglect the stresses in the air above the layer and assume its density to be zero we can take the pressure at the free surface to be zero. The conditions at the free surface, including the effects of surface tension, are then

$$(\bar{U}_{\hat{X}} - \hat{V}_y)\eta + \tfrac{1}{2}(\bar{U}_y + \hat{V}_{\hat{X}})(1-\eta_{\hat{X}}^2) = 0, \tag{2.2a}$$

$$s\bar{P} = \frac{2}{Re(1+\eta^2)}[\bar{U}_{\hat{X}}\eta_{\hat{X}}^2 - (\bar{U}_y + \hat{V}_{\hat{X}})\eta_{\hat{X}} + \hat{V}_y] - \frac{Ts}{\rho g h^{*2}}\frac{\eta_{\hat{X}\hat{X}}}{(1+\eta_{\hat{X}})^{\frac{3}{2}}}, \tag{2.2b}$$

$$\bar{U}\eta_{\hat{X}} = \hat{V}. \tag{2.2c}$$

Here T is the coefficient of surface tension of the fluid/air interface. We now assume that the lengthscale of the adjustment of the layer is long compared with its depth and make the boundary-layer approximation. More specifically we scale $\hat{X}$ with Re ($\hat{X} = xRe$) and $\hat{V}$ with Re^{-1} ($\hat{V} = Re^{-1}\bar{V}$) and let $Re \to \infty$. Surface tension effects will be important over these scales if $Ts/\rho g h^{*2} Re^2$ is $O(1)$ as $Re \to \infty$. For the moment we will presume that this is not the case. If we now write

$$s\bar{P} = -s(y-1) + p, \tag{2.3}$$

and neglect surface tension, we are led to the system

$$\bar{U}\bar{U}_x + \bar{V}\bar{U}_y = -p_x + \bar{U}_{yy}, \tag{2.4a}$$

$$\bar{U}_x + \bar{V}_y = 0, \tag{2.4b}$$

$$\int_0^{1+\eta} \bar{U}(y)\,dy = 1, \tag{2.4c}$$

$$\bar{U} = \bar{V} = 0 \quad \text{at} \quad y = 0, \tag{2.4d}$$

$$\bar{U}_y = 0 \quad \text{at} \quad y = 1+\eta, \tag{2.4e}$$

$$p_y = 0, \quad p = s\eta, \tag{2.4f, g}$$

$$\bar{U} = \bar{U}_0(y), \quad \eta = 0 \quad \text{as} \quad x \to -\infty. \tag{2.4h}$$

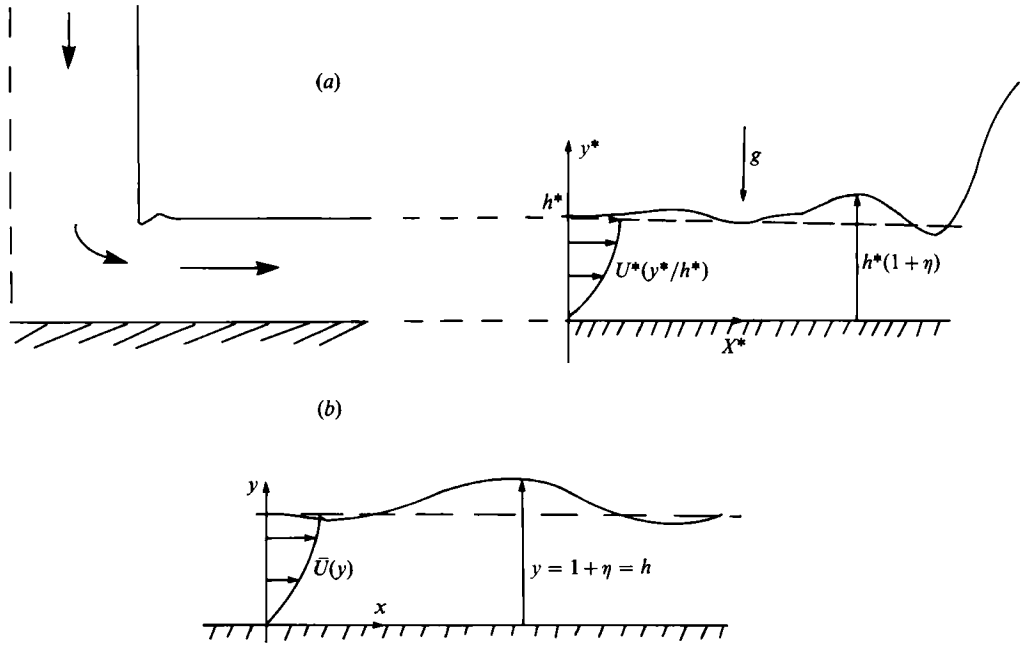

FIGURE 2. Diagrammatical sketches of the hydraulic jump problem as described near the start of §2.1: (*a*) the problem in dimensional terms, (*b*) the problem associated with equation (2.4).

Equations (2.4) are the equations governing the development of the liquid layer over a long $O(Re)$ lengthscale. They are interactive in that the pressure driving the layer is not prescribed but is determined by the interaction of the viscous forces throughout its depth and the unknown position of the free surface. If we suppress the interaction by setting s identically equal to zero we obtain equations corresponding to those studied by Watson.

2.2. *Large Froude numbers and shorter scales*

The case of finite s has been studied by Bowles (1990). The interaction is then strongly influenced by effects associated with the non-parallelism of the basic flow. However at large Froude numbers, i.e. small s, the lengthscale of the interaction is found below to shorten to $O(Res^3)$ and the governing equations, at first, become essentially those studied by Gajjar & Smith (1983).

To show this we seek a perturbation to the oncoming flow of the following form, with $\bar{U} = \bar{\psi}_y$:

$$\bar{\psi} \sim \bar{\psi}_0 + s\bar{\psi}_1, \quad \eta \sim \eta_0 + s\eta_1, \quad p \sim sp_0 + s^2 p_1, \tag{2.5a–c}$$

where $\bar{\psi}_0, \eta_0, p_0$ represent the oncoming flow and are functions of x satisfying (2.4*a–h*), see figure 3. Without loss of generality we can let η_0 be zero so that the depth of the layer is initially unity. In addition, therefore, $p_0 = \eta_0 = 0$. The perturbation quantities, $\bar{\psi}_1, \eta_1, p_1$ are functions of the fast variable $\hat{x} = x/s^3$ and $p_1 = \eta_1$. In the main part of the flow where $y \sim O(1)$ (region I in figure 3) the rapid growth of the perturbation dominates and the solution is governed by inertial effects, with the pressure term reduced in importance by the smallness of s. Therefore (2.4*a–h*) reduce here to

$$\bar{\psi}_0' \bar{\psi}_{1\hat{x}}' - \bar{\psi}_0'' \bar{\psi}_{1\hat{x}} = 0, \tag{2.6}$$

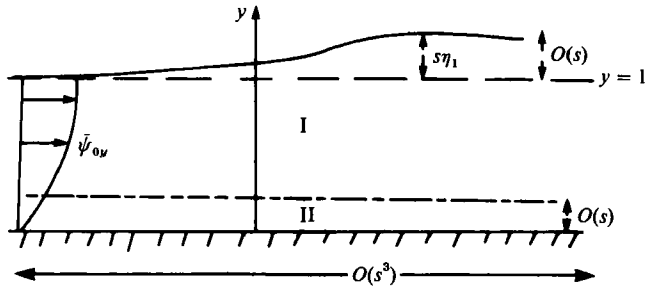

FIGURE 3. The structure of the free interaction for large Froude number (s^{-1}).

where a prime indicates differentiation with respect to y. This result neglects cross-stream pressure gradients (arising from the $\bar{U}\hat{V}_{\hat{x}}$ term in (2.1b)) with a relative error of $O(s^{-7}Re^{-2})$. It has solution $\bar{\psi}_1 = A_1(\hat{x})\bar{\psi}_0'$. Application of the boundary conditions at the free surface which, neglecting surface tension effects, reduce to $\bar{\psi}_1(1) = -\eta_1'\bar{\psi}_0'(1)$ and $\bar{\psi}_1''(1) = -\eta_1\bar{\psi}_0(1)$, yields

$$A_1 = -\eta_1 = -p_1. \tag{2.7}$$

As $y \to 0$ we obtain, if $\bar{\psi}_0 \sim \frac{1}{2}\lambda y^2$,

$$\bar{\psi} \sim \tfrac{1}{2}\lambda y^2 + sA_1\lambda y, \tag{2.8}$$

so a sublayer (region II in figure 3) of thickness $y \sim O(s)$ is produced at the wall to reduce the resulting slip velocity, $sA_1\lambda$, to zero. Here we write $y = s\hat{z}$ and $\bar{\psi} = s^2\tilde{\psi}(\hat{z})$, $\bar{U} \sim s\tilde{U}(\hat{z})$, where $\tilde{U} = \tilde{\psi}_{\hat{z}}$, and so we obtain a nonlinear inertia–viscosity–pressure balance in this sublayer,

$$\tilde{U}\tilde{U}_{\hat{x}} - \tilde{\psi}_{\hat{x}}\tilde{U}_{\hat{z}} = -p_{1\hat{x}} + \tilde{U}_{\hat{z}\hat{z}}, \tag{2.9a}$$

$$\tilde{U} = \tilde{\psi}_{\hat{z}}, \tag{2.9b}$$

$$\tilde{U}(0) = \tilde{\psi}(0) = 0, \tag{2.9c}$$

$$\tilde{U} \sim \lambda(\hat{z} + A_1), \quad \hat{z} \to \infty, \tag{2.9d}$$

$$\tilde{U} \sim \lambda\hat{z}, \quad \hat{x} \to -\infty, \tag{2.9e}$$

and, from (2.7),

$$p_1 = -A_1 \tag{2.9f}$$

The above result is true for small s. These equations are, in fact, identical to those derived by Gajjar & Smith and predict, as described in the introduction, a blunt jump profile.

The above analysis shows that the interaction can also take place in layers with a general velocity profile provided that the Froude number is sufficiently large. So the application here is a broad one.

2.3. *Surface tension and curvature*

The lengthscale of the interaction has shortened from $O(Re)$ to $O(s^3Re)$ and this means that the neglected curvature effects are no longer small. They appear to first order if $s = Re^{-\frac{1}{7}}\bar{s}$ and $Ts/\rho gh^{*2} = \bar{T}$, say, where $\bar{s}$ and $\bar{T}$ are $O(1)$ as $Re \to \infty$. If this is the case then $T/\rho gh^{*2} = \bar{T}/\bar{s}Re^{\frac{3}{7}}$. The lengthscale of the interaction is then $O(Re^{\frac{1}{7}})$, which is the scale associated with upstream influence in boundary-layer jets, see Smith & Duck (1977), or channel flow, see Smith (1976a, b), when it is streamline curvature which is the dominant inviscid effect. If we repeat the above argument on

this lengthscale and with the above definitions of $\bar{T}$ and $\bar{s}$ we find the following additional equations holding in region I:

$$p_1|_{y=1} = \bar{T}\bar{s}^{-7}A_{1\hat{x}\hat{x}} - A_1, \quad p_{1y} = \bar{s}^{-7}A_{1\hat{x}\hat{x}}\bar{\psi}_0'^2, \tag{2.10a, b}$$

so that,

$$p_1|_{y=0} = -A_1 + \bar{s}^{-7}\left(\bar{T} - \int_0^1 \bar{\psi}_0'^2\,\mathrm{d}y\right)A_{1\hat{x}\hat{x}}, \tag{2.10c}$$

instead of (2.9*f*). We can normalize this set of equations further by factoring out λ, the value of $\bar{\psi}_0''(0)$. Thus we find

$$UU_X + VU_Y = -P_X + U_{YY}, \tag{2.11a}$$

$$U_X + V_Y = 0, \tag{2.11b}$$

$$U = V = 0 \quad \text{at} \quad Y = 0, \tag{2.11c}$$

$$U \to Y + A \quad \text{as} \quad Y \to \infty, \tag{2.11d}$$

$$A \to 0 \quad \text{as} \quad X \to -\infty, \tag{2.11e}$$

$$P = -A + \gamma A_{XX}. \tag{2.11f}$$

Here,

$$\gamma = \frac{\lambda^{10}\int_0^1 \bar{\psi}_0'^2\,\mathrm{d}y}{Re^2 s^7}(\mu - 1), \quad \mu = \frac{sT}{\rho g h^{*2}\int_0^1 \bar{\psi}_0'^2\,\mathrm{d}y}, \tag{2.12a, b}$$

the lengthscale over which the interaction occurs is

$$L^* = h^* s^3 Re/\lambda^5, \tag{2.12c}$$

and the position of the free surface alters by an amount

$$\delta h^* = h^*(s/\lambda^2)(-A). \tag{2.12d}$$

Surface-tension effects dominate those of streamline curvature if γ is positive. This is the case in the experiments. We note here that the downstream asymptote for the case studied by Gajjar & Smith (1983) ($\gamma = 0$) is still valid for the case $\gamma \neq 0$, sufficiently far downstream, and capillary influence is effective over a relatively short lengthscale: see below. Therefore (2.11) is found to predict a jump whose downstream form is dominated by the gravitational term ($-A$), but whose upstream form is greatly affected by the surface tension term (γA_{XX}), as shown in the following two sections.

3. Linear solutions

As a first step in understanding the solutions of (2.11), we will solve them for a flow over a small obstacle, $y^* = \Delta h^* Re^{-\frac{3}{7}}\bar{s}\lambda^{-2}F$ with $\Delta \ll 1$. We write

$$(U - Y, V, P, A) = \Delta(u, v, p, a), \tag{3.1}$$

with u, v, p, a $O(1)$ as $\Delta \to 0$. After a Prandtl transformation the governing equations are

$$Yu_X + v = -p_X + u_{YY}, \tag{3.2a}$$

$$u_X + v_Y = 0, \tag{3.2b}$$

$$u \sim a + F \quad \text{as} \quad Y \to \infty, \tag{3.2c}$$

$$u = v = 0 \quad \text{at} \quad Y = 0, \tag{3.2d}$$

$$p = -a + \gamma a_{XX}. \tag{3.2e}$$

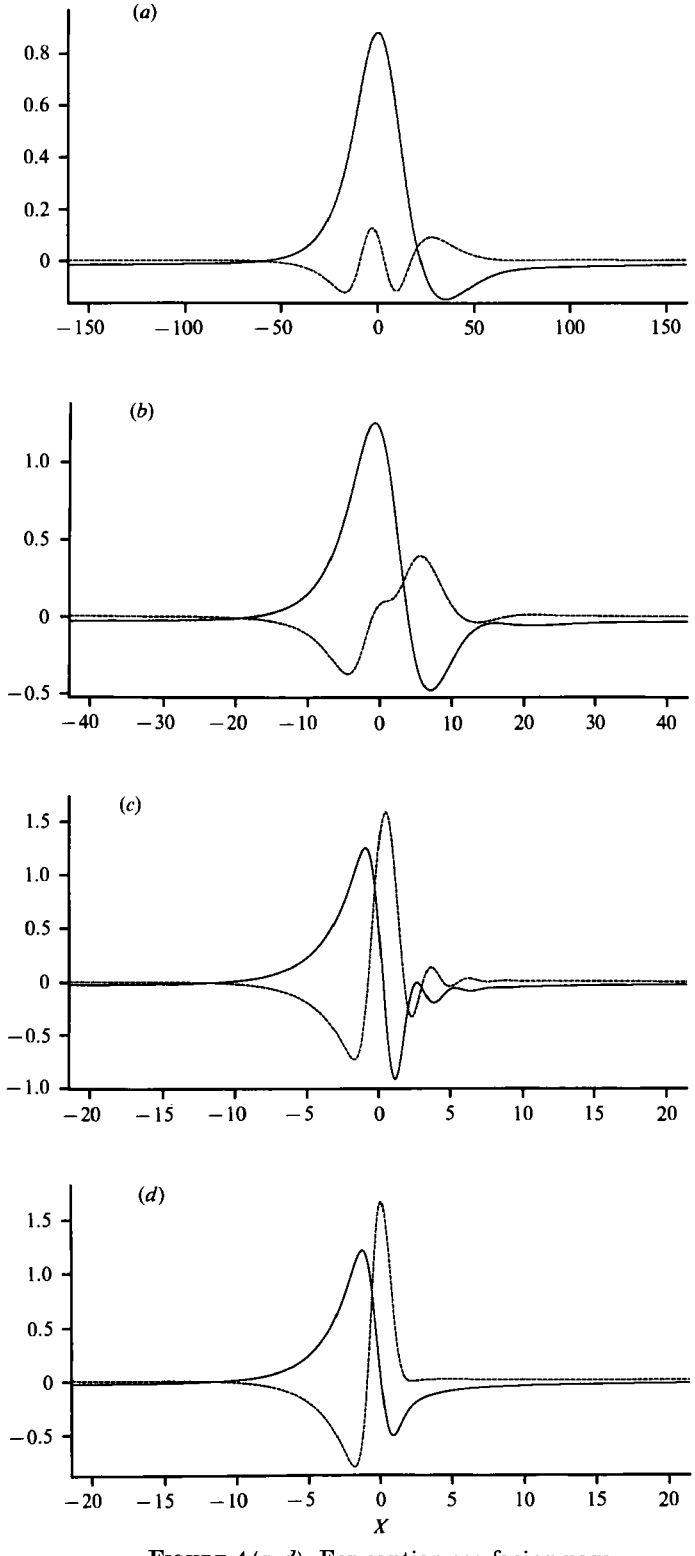

FIGURE 4 (*a–d*). For caption see facing page.

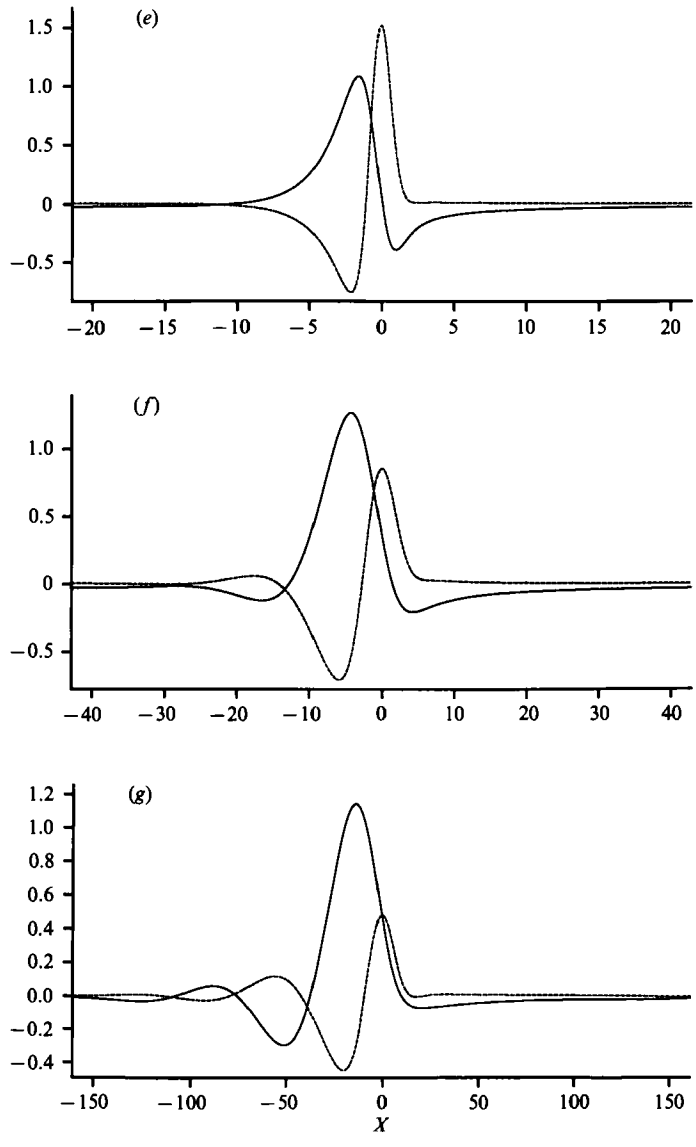

FIGURE 4. Solutions for linearized flow over an obstacle. Changes in free-surface position (——) and skin friction (– –) for flow over the obstacle (3.5*a*) for $\gamma = -100, -3, -0.1, 0, 0.1, 3, 100$, $l = 10, 3, 1, 1, 1, 3, 10$ for cases (*a–g*) respectively.

We solve these by means of Fourier transforms in X where the transform $\hat{g}$ of g is defined by

$$\hat{g} = \frac{1}{(2\pi)^{\frac{1}{2}}} \int_{-\infty}^{\infty} \mathrm{e}^{-\mathrm{i}kX} g \, \mathrm{d}x, \tag{3.3}$$

and find

$$\hat{a} = -\frac{\hat{F}}{1-\sigma(\mathrm{i}k)^{\frac{1}{3}}(1+\gamma k^2)}, \tag{3.4a}$$

$$\widehat{u_Y|_0} = -\frac{\mathrm{Ai}_0}{|\mathrm{Ai}_0'|} \frac{\hat{F}(\mathrm{i}k)^{\frac{2}{3}}(1+\gamma k^2)}{1-\sigma(\mathrm{i}k)^{\frac{1}{3}}(1+\gamma k^2)}, \tag{3.4b}$$

where
$$\sigma = 1/3|\mathrm{Ai}_0'|, \tag{3.4c}$$
$$-\tfrac{1}{3}\pi < \arg(\mathrm{i}k)^{\frac{1}{3}} \leqslant \tfrac{1}{3}\pi, \tag{3.4d}$$

and Ai_0 is the value of Airy's function evaluated at zero. The value of σ is approximately 1.288.

We will consider the exponential hump,

$$F = \exp(-X^2/l^2), \qquad \hat{F} = \frac{l}{\sqrt{2}}\exp(-\tfrac{1}{2}k^2l^2). \tag{3.5a, b}$$

These expressions are inverted using a fast Fourier transform routine and the results are shown in figure 4. It can be seen that for positive γ, which corresponds to surface tension effects dominating those of streamline curvature, the upstream behaviour is wave-like due to upstream capillary waves. The waves are not present for smaller values of γ. If γ is positive there are waves just downstream of the obstacle and none upstream. Another feature of note is the increase in the scale of the upstream influence as $|\gamma|$ increases. In interpreting these results it is helpful to have some knowledge of the poles and branch cuts associated with the integrand.

We begin by discussing the behaviour downstream of the obstacle, determined by the features in the upper half of the complex k-plane. There is a branch cut running from the origin to $+\mathrm{i}\infty$ and this, viscous, phenomenon is responsible for the algebraic decay (like $X^{-\frac{1}{3}}$) at downstream infinity. For non-negative γ there are no poles in this half-plane and the above decay is the only feature. However, if γ is negative and the effects of streamline curvature dominate those of surface tension there are poles and wave-like behaviour is seen. As $|\gamma|$ increases from zero these poles migrate from

$$k = \pm\frac{1}{|\gamma|^{\frac{1}{2}}} + \frac{1}{2\sigma|\gamma|^{\frac{1}{3}}}\exp(\tfrac{1}{2}\pi\mathrm{i} \pm \tfrac{1}{3}\pi\mathrm{i}), \tag{3.6}$$

to
$$k = \frac{1}{(\sigma|\gamma|)^{\frac{3}{7}}}\exp(\tfrac{1}{2}\pi\mathrm{i} \mp \tfrac{1}{7}\pi\mathrm{i}). \tag{3.7}$$

If $|\gamma|$ is small there is an interaction between the gravitational term in (2.11f) ($-A$) and the curvature term (A_{XX}). This gives rise to short gravity waves. The interaction of these waves with the boundary layer near the wall is less important but, nevertheless, still gives rise to a rapid decay of the waves downstream. As curvature begins to dominate over gravity these waves become more of a viscous–inviscid interaction and become long and more rapidly decaying, relative to their length.

Upstream the solution is influenced by the lower half-plane. If γ is identically zero there is a pole at $k = -\mathrm{i}\sigma^{-3}$ and this gives rise to the smooth exponential upstream influence seen in the results. For small γ another root appears on the negative imaginary axis, which, like that for small negative γ, has its origin in an inviscid interaction between capillary effects and gravity. This pole is at

$$k = -\mathrm{i}\left(\frac{1}{\gamma^{\frac{1}{2}}} - \frac{1}{2\sigma\gamma^{\frac{1}{3}}}\right). \tag{3.8}$$

It corresponds to a short-scale upstream effect and is not seen in the calculations (see the discussions in §4). As γ increases these two eigensolutions approach one another and merge to give rise to oscillatory upstream influence if $\gamma > 0.257$. These waves are caused by gravitational, capillary and viscous effects and are initially long compared

with the upstream-influence lengthscale. As γ increases further, upstream waves become more obvious. Finally for large γ there are long waves governed primarily by surface tension and viscosity and associated with poles at

$$k = \frac{1}{(\sigma\gamma)^{\frac{3}{7}}} \exp\left(\tfrac{6}{7}n\pi\mathrm{i} - \tfrac{1}{14}\pi\mathrm{i}\right), \quad n = 0, -1. \tag{3.9}$$

So, for linearized disturbances at least, the inclusion of capillary effects in the theory of Smith & Gajjar has the effect of allowing the upstream influence to be wave-like. This feature of the interaction is seen in the experiments of Craik *et al.* The next section gives the results of integrating the fully nonlinear equations for the problem of a free interaction.

4. The free interaction: computational solutions and analysis

The previous section describes linearized solutions and predicted the upstream response of the supercritical liquid layer to a small obstacle. As the size of the obstacle is increased we expect the extent of the upstream influence to increase and eventually separation to occur ahead of the obstacle. As the obstacle size is increased further we would see the separation occurring far ahead of the obstacle as a result of a free interaction. In the present context we interpret this as a hydraulic jump upstream of the obstacle. It must be emphasized that the downstream conditions retain an influence on the position of this free interaction, see Smith (1982).

Computational solutions of the free interaction (2.11) were obtained, for various γ-values, by a finite-difference scheme of the box type, which is now fairly standard and so does not require a detailed description here. The scheme is nominally second-order accurate. The interaction is started with a small positive or negative pressure kick, upstream, leading downstream to a nonlinear response which is tracked by forward-marching in X and using Newton iteration at each X-station. Typically the values taken for the grid sizes $\Delta X, \Delta Y$, in X, Y respectively, were 0.05–0.2, the iterative tolerance was 10^{-7}, and the outer-edge value of Y was $Y_\infty = 5$–20; grid-effect studies suggest that these values are satisfactory for graphical accuracy at least. At $Y = Y_\infty$ the two constraints (cf. (2.11*d*))

$$U = Y_\infty + A, \qquad \tau = 1, \tag{4.1a, b}$$

are imposed, where $\tau = U_Y$, to avoid exponential growth in Y in effect, and (4.1) is coupled with the interaction law (2.11*f*), written in the form

$$B = A_X, \qquad P = -A + \gamma B_X, \tag{4.2a, b}$$

for convenience. Here (4.2) is discretized using two-point formulae centred midway between the current X-station and the previous one. When reversed flow is encountered, beyond the regular separation point at which $\tau_w = \tau(X, 0)$ vanishes, the FLARE technique is employed, i.e. the term UU_X is neglected wherever $U < 0$, as an extra approximation to help stabilize the forward march. See also the comments in Gajjar & Smith and later in this section.

The free-interaction results obtained are summarized in figures 5 and 6, covering a range of values of $\gamma \geqslant 0$. For zero γ there are basically two options for the free interaction, corresponding to a positive or a negative upstream pressure kick. The former gives the solution of Gajjar & Smith (1983), leading to separation downstream, whereas a negative kick yields the Brown, Stewartson & Williams (1975) solution

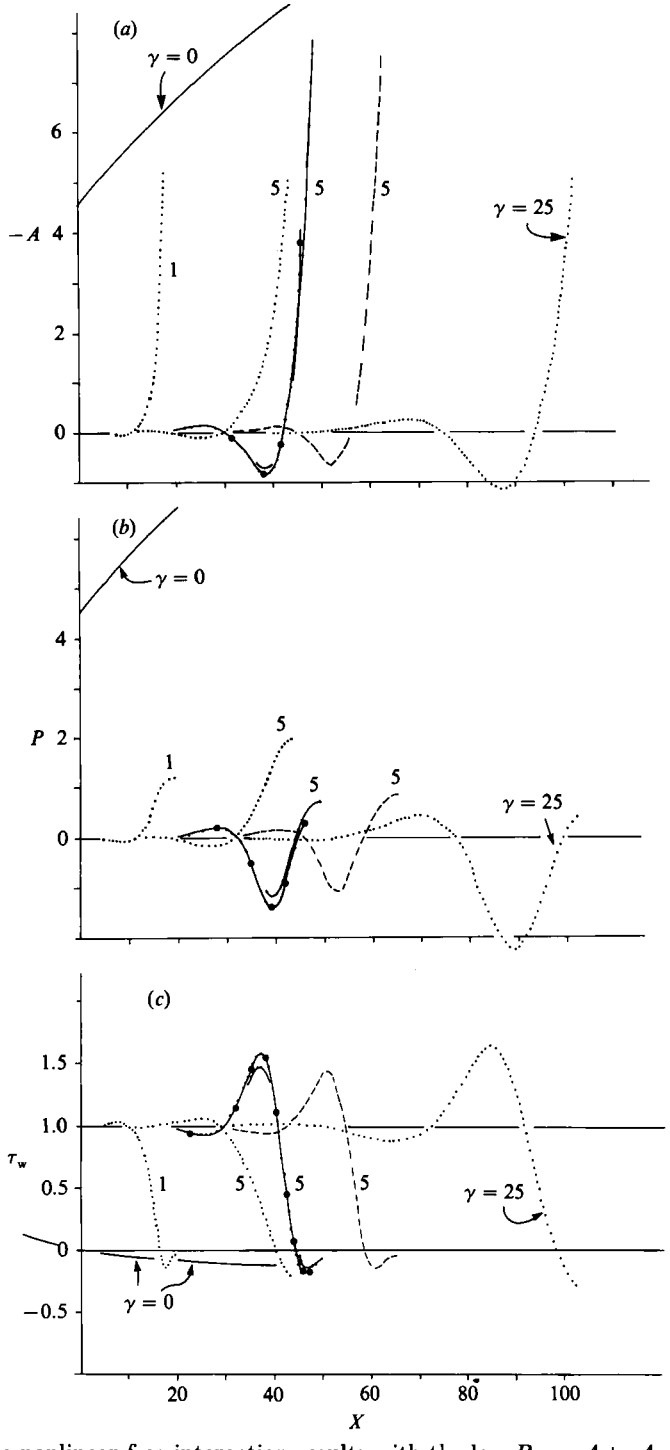

FIGURE 5. The nonlinear free-interaction results with the law $P = -A + \gamma A_{XX}$, for various values of $\gamma \geqslant 0$, showing (*a*) $-A$, (*b*) P, (*c*) τ_w, versus X. The pressure kicks used for the curves (left to right) in order were 0.0001, 0.001, −0.001, 0.001, −0.0001, −0.001. The results marked ● show the influence of increasing Y_∞ to 10. The curve for $\gamma = 0$ has an origin shift of 50 in X.

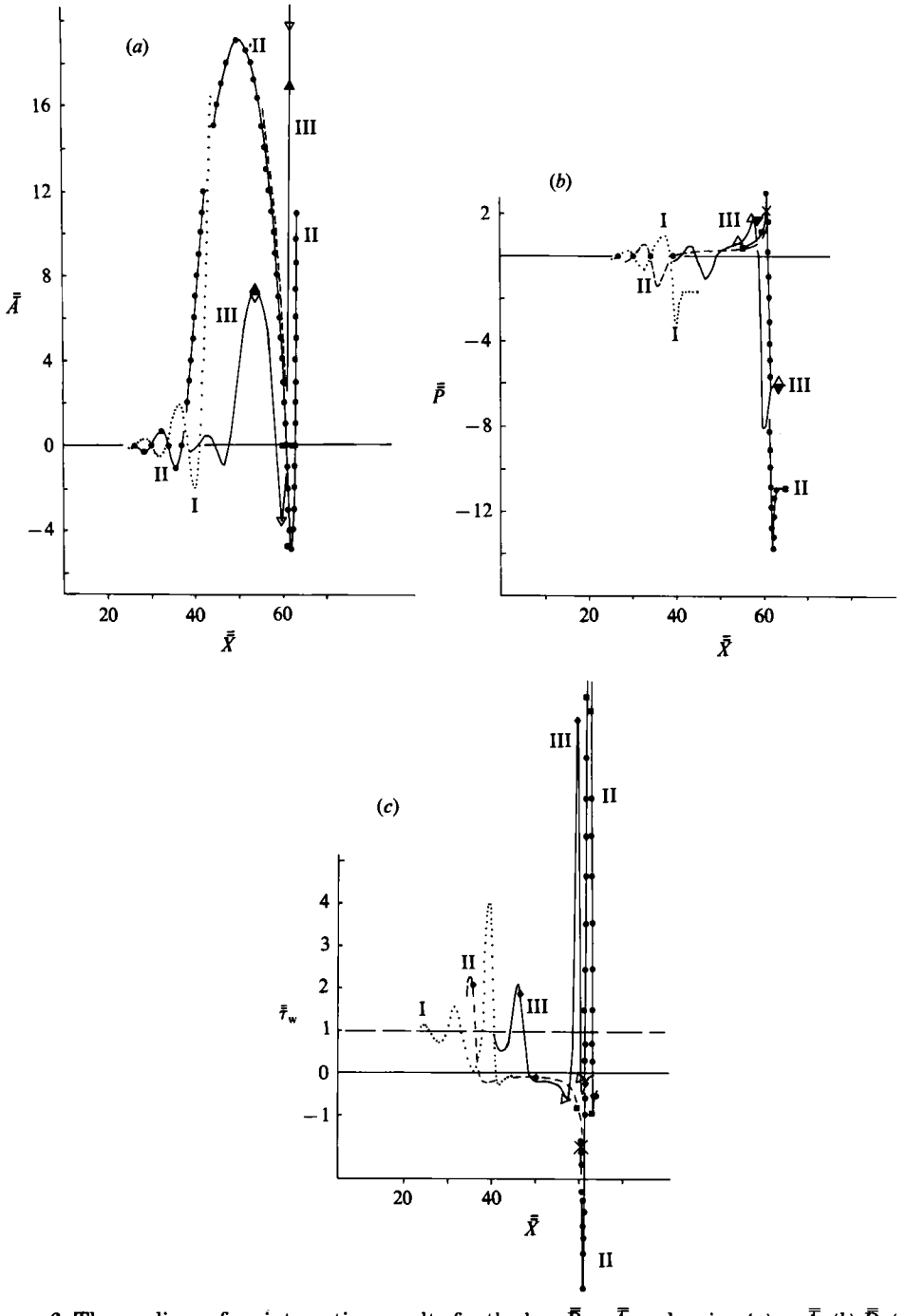

FIGURE 6. The nonlinear free-interaction results for the law $\bar{P} = \bar{A}_{\bar{X}\bar{X}}$ showing (*a*) $-\bar{A}$, (*b*) $\bar{P}$, (*c*) $\bar{\tau}_w$, versus $\bar{X}$, obtained from pressure kicks 0.001, −0.001, 0.0001, upstream (I, II, III, respectively). Here the results denoted ●, △, ▼, ■ indicate the typical effects of halving or doubling $\Delta\bar{Y}$ or $\Delta\bar{X}$; otherwise $(\bar{Y}_\infty, \Delta\bar{Y}, \Delta\bar{X}) = (40, 0.2, 0.05)$.

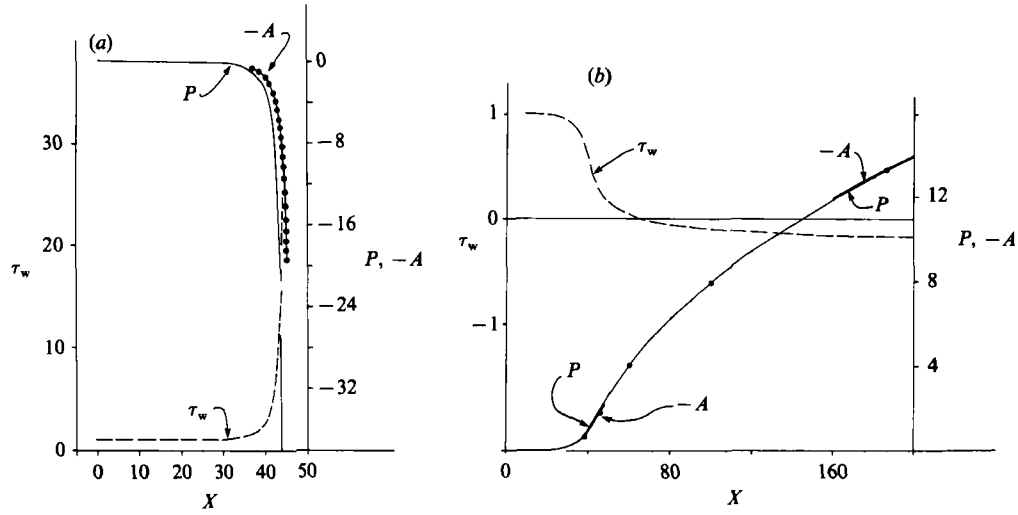

FIGURE 7. Typical results for the nonlinear free-interaction with the law $P = -A + \gamma A_{XX}$ but negative γ, showing $-A$, P, τ_w, versus X. Here $\gamma = -5$, $(Y_\infty, \Delta Y, \Delta X) = (40, 0.2, 0.05)$, with ● showing the effects of doubling Y_∞; the upstream pressure kicks are (*a*) −0.0001, (*b*) 0.0001.

which terminates in a strong attaching-flow singularity at a finite X-station. In contrast, for positive γ there is in broad terms only one kind of non-trivial free interaction, that leading to separation downstream, for any sign of the pressure kick upstream. This 'uniqueness' is supported, first, by the computational results in figures 5 and 6 for pressure kicks of different signs, where downstream separation is always found. In fact, one could argue that, because of the wave-like exponential form upstream, infinitely many nonlinear free interactions can be provoked by varying the kick, subject to a periodicity property, and some examples are shown in the figures. All the resulting interactions are believed to end up with separation downstream, however. The 'uniqueness' is supported, second, analytically, by the property that a finite-distance singularity (at $X = X_0$ say) associated with strong attachment requires both A and $-P$ to become large and positive, essentially because of a dominant inviscid Bernoulli balance ($P = -\frac{1}{2}A^2$) and induced slip velocity ($\approx A$) which must be positive for consistency as $X \to X_0-$; but the interaction law (2.11*f*) is then dominated by $P \approx \gamma A_{XX}$ locally near $X = X_0-$, a form which clearly requires A and P to have the same sign (in a singularity) and thus contradicts the above. So a finite-distance singularity seems to be ruled out. If γ were negative, by the way, such a singularity would be attainable, of the form in Smith (1977) with $P \propto (X-X_0)^{-4}$ and $A \propto (X-X_0)^{-2}$; see §6 and figure 7.

It follows that, although the contribution γA_{XX} in (2.11*f*) with γ positive still allows upstream influence to be present (and in a wave-like exponential form, as in the linear upstream solutions in §3), the subsequent nonlinear behaviour downstream is distinct from that found in all previous free-interaction studies, as far as we know. The initially small wave-like disturbances upstream develop to produce nonlinear spatial oscillations, as shown in A, P, τ_w in the figures. These oscillations increase in magnitude downstream, as, typically, a rising pressure (adverse gradient) forces the skin friction τ_w to decrease and the scaled displacement effect ($-A$) to increase, forcing the curvature $-A_{XX}$ up and hence the surface-tension pressure γA_{XX} down, which can eventually overwhelm the gravity pressure and so tends to lead on next to a favourable pressure gradient followed by increasing τ_w and decreasing $-A$,

hence eventually raising the surface-tension pressure, and so on as the downstream distance increases. A final nonlinear oscillation causes the flow to separate (τ_w becomes negative), under an adverse pressure gradient, in the cases in figure 6. After that, the numerical evidence rather tends to suggest that the flow solution stays separated and acquires a breakaway-separation structure far downstream, as described below. We should remark here however that, on the one hand, the computational scheme usually failed not far beyond the separation point, as is quite often the case for forward-marching calculations for reversed motions (multi-sweeping with windward-differencing would be better, in principle), and on the other hand it is not unlikely that more nonlinear oscillations could occur for some cases, yielding one or even more reattachments downstream: see the third paragraph below. Again, all the results at stations beyond the separation point should be viewed with caution because of the reversed direction of influence here, as discussed further subsequently.

The physically acceptable far-downstream response of all the free interactions with $\gamma \geqslant 0$ appears to be controlled at leading order by the $-A$ term, as opposed to the γA_{XX} one, in the interaction law (2.11f), simply because X is large and positive. Hence the asymptotes have the form

$$P \sim P_1 X^m + \ldots, \qquad -A \sim P_1 X^m + \ldots, \tag{4.3a, b}$$

from Gajjar & Smith; see the values of P_1, m in §1. Only higher-order terms are affected by the γA_{XX} contribution. Thus the downstream asymptote is dominated by the gravity-induced pressure, with the surface-tension effect playing a secondary role there. There is an alternative downstream response which is of possible physical interest, namely that

$$P \sim \text{constant}, \qquad -A \sim \exp(\gamma^{-\frac{1}{2}} X), \tag{4.3c, d}$$

at large positive X. Here the balance between gravity and surface-tension effects in (2.11f) persists downstream, forcing, for positive γ exponential breakaway as in (4.3d), and the separated flow structure produced is essentially the same as in Smith (1978). It so happens that the present computational results appear to tie in with (4.3c, d) rather than (4.3a, b), as X increases beyond separation, and indeed the quantitative agreement is found to be very close. We should recall that the interaction problem is really an elliptic one, with or without separation present, and so the far-downstream conditions can affect the whole interaction and in particular suppress exponential downstream growth; this is shown analytically by Bowles (1990) for some related nonlinear interactive flows without separation. With separation occurring, in the present context, the entire flow solution beyond the separation point depends directly on the reversed-flow properties downstream, including especially the vorticity distribution there (see also the next paragraph concerning the reversed velocity profiles). The forward-marching computational solutions described above can take no account of this direct mechanism of upstream influence beyond separation and so, as with all other treatments of free-interaction separations, the computational solutions must be regarded with considerable caution, and in strict terms are invalid, beyond separation. The favoured case, in view of these points is that of (4.3a, b) although the exponential increase (4.3c, d) may be of relevance for certain downstream conditions (cf. a near-stationary solitary wave of the type described by Benjamin 1962).

The same conclusion holds true even when γ is large (an extreme which is of much interest with regard to the experimental comparisons in the next section). Then the

free interaction splits into two parts, in essence. The first part, upstream, has the gravity effect $-A$ negligible compared with the surface-tension effect γA_{XX}, so that with the scaling transformation

$$(U, V, P, A, X, Y) = (\gamma^{\frac{1}{7}}\bar{U}, \gamma^{-\frac{1}{7}}\bar{V}, \gamma^{\frac{2}{7}}\bar{P}, \gamma^{\frac{1}{7}}\bar{A}, \gamma^{\frac{3}{7}}\bar{X}, \gamma^{\frac{1}{7}}\bar{Y}), \tag{4.4}$$

applied the governing equations remain as in (2.11), with double overbars added, except that the interaction law becomes

$$\bar{\bar{P}} = \bar{\bar{A}}_{\bar{\bar{X}}\bar{\bar{X}}}. \tag{4.5}$$

The correction term due to gravity is of the order $\gamma^{-\frac{1}{7}}$. The appearance of the $\frac{1}{7}$ powers in (4.4) is consistent with that of the $\frac{1}{7}$ powers of the Reynolds number in the original scalings used in §2, and in particular the largeness of γ tends to prolong the free interaction (as is evident from figure 5), in contrast to the influence of the large Froude number described in §2. The solutions for the case (4.5) are presented in figure 6. The previous comments in this section, regarding the wave-like upstream influence, the 'uniqueness' of the downstream response as the upstream pressure kick is varied and the dynamics of the nonlinear oscillations, apply here also, by and large, the exception being the downstream asymptote for the breakaway separating motion, Here, at large positive $\bar{\bar{X}}$, a pressure plateau is approached with

$$\bar{\bar{P}} \to \bar{\bar{P}}_\infty, \qquad -\bar{\bar{A}} \sim \tfrac{1}{2}(-\bar{\bar{P}}_\infty)\bar{\bar{X}}^2, \tag{4.6a, b}$$

giving the scaled pressure and displacement properties. This response is analogous with the result of Smith & Duck (1977) for jet–flow interactions (in which $\bar{\bar{P}} = -\bar{\bar{A}}_{\bar{\bar{X}}\bar{\bar{X}}}$), except that in the present case $\bar{\bar{P}}_\infty$ must be negative and is non-unique; see figure 6. The separated-flow structures associated with (4.3a, b), (4.6) are similar to some extent, each having an $O(X^{\frac{1}{3}})$ (or $O(\bar{\bar{X}}^{\frac{1}{3}})$) detached shear layer above a reversed-flow sub-boundary-layer at the surface, although the reversed velocity profiles in the inviscid region are non-uniform and uniform respectively, and algebraic growth of the solution in the sub-boundary-layer is present in (4.3a, b) but not for (4.6). Again with regard to the current case (4.6), there is a certain novelty to note here, in the sense that downstream breakaway separation is produced by an overall fall in the pressure!

Another interesting novel feature seen in figure 6 is that, depending on the initial pressure kick, free interactions can encounter a reversed flow region of finite extent, prior to the ultimate breakaway separation that leads to (4.6). This short-bubble phenomenon, involving separation, then reattachment, and then separation again, is mentioned further in §6. The first separation leaves the pressure $\bar{\bar{P}}$ becoming positive (cf. (4.6a)), so that the displacement then curves downwards eventually (from (4.5)), causing the subsequent reattachment, after which the second separation leaves $\bar{\bar{P}}$ negative, in readiness for the ultimate behaviour of (4.6a) further downstream. A similar short-bubble phenomenon could occur for γ of $O(1)$ also, as mentioned previously.

The second part of the large-γ interaction arises further downstream, where

$$X \sim \gamma^{\frac{1}{7}}, \tag{4.7}$$

and the effects of the gravity term return to leading order. This is due to the downstream growth of the gravity-induced pressure, like distance squared from (4.6b), compared with the plateau in the surface-tension pressure (4.6a), and it can be inferred directly from (2.11f) also. The crossover, from the first asymptote (4.6) to that of (4.3a, b) further downstream, occurs within the scale of (4.7) and is similar

to that described by Smith (1985). The crossover is effectively one from surface-tension-dominated interaction to gravity-dominated interaction. A similar division of the free interaction into an upstream region where surface tension dominates and a second, downstream, region where gravity is the dominant effect, occurs in the case studied by Bowles (1990), of low-Froude-number liquid-layer flow down a shallow incline under the influence of relatively strong surface-tension effects.

Concerning comparisons between the free-interaction computations for increasing γ in figure 5 and those for the large-γ limit in figure 6, the approach to the limit seems to be relatively slow, probably because of the $O(\gamma^{-\frac{1}{7}})$ correction, mentioned just after (4.5). Nevertheless the comparisons tend to be affirmative overall in qualitative terms. A broadly similar comment applies to the comparisons with the asymptotes (4.3*a*, *b*) and (4.6*a*, *b*) (granted the reservations expressed earlier concerning the results in the reversed-flow regions), although the latter appears to be emerging fairly clearly in the results of figure 7 which illustrates the case of negative γ, in which the asymptotes (4.3*c*, *d*) are not attainable.

The above theory, therefore, seems to capture much of the structure seen in the experiments of Craik *et al.* the wave-like upstream influence caused by capillary effects, and the eventual large jump itself where the gravity-induced pressure is dominant. We now move on to compare quantitatively the theory with the experimental results.

5. Comparisons with experiments

5.1. *The flow upstream of the hydraulic jump*

Our suggestion is that the circular hydraulic jumps described in the introduction are free, viscous–inviscid interactions, of the type described in §4 forced by an unspecified downstream condition and following an incident fully developed flow.

We believe for two reasons that the flow is fully developed at the position of the jump. First, the Froude numbers of the layers in the experiments are large, typically between 20 and 50. The development is therefore likely to be governed by Watson's solution which assumes an infinite Froude number and predicts, in this axisymmetric case, a quadratic growth in the depth of the layer. This growth agrees qualitatively with that seen in figure 1. The depth just upstream of the jump position, predicted with this assumption, is much closer to the measured values than those predicted by inviscid theory. Watson's theory is, however, only asymptotically correct far downstream and so the origin of the expansion is unknown. Watson makes an approximation to the unknown constant in the solution using the Kármán–Pohlhausen method. We prefer to integrate the equations numerically. The results provide the second reason, namely that the flow predicted by the numerical solution is indeed fully developed and given by Watson's solution at the jump position. The equations governing the large-Froude-number axisymmetric flow are

$$(x^*U^*)_{x^*} + (x^*V^*)_{y^*} = 0, \tag{5.1a}$$

$$U^*U^*_{x^*} + V^*U^*_{y^*} = \nu U^*_{y^*y^*}, \tag{5.1b}$$

$$2\pi x^* \int_0^{h^*} U^* \,\mathrm{d}y^* = Q, \tag{5.1c}$$

$$U^* = V^* = 0 \quad \text{at} \quad y^* = 0, \tag{5.1d}$$

$$U^*_{y^*} = 0 \quad \text{at} \quad y^* = h^*. \tag{5.1e}$$

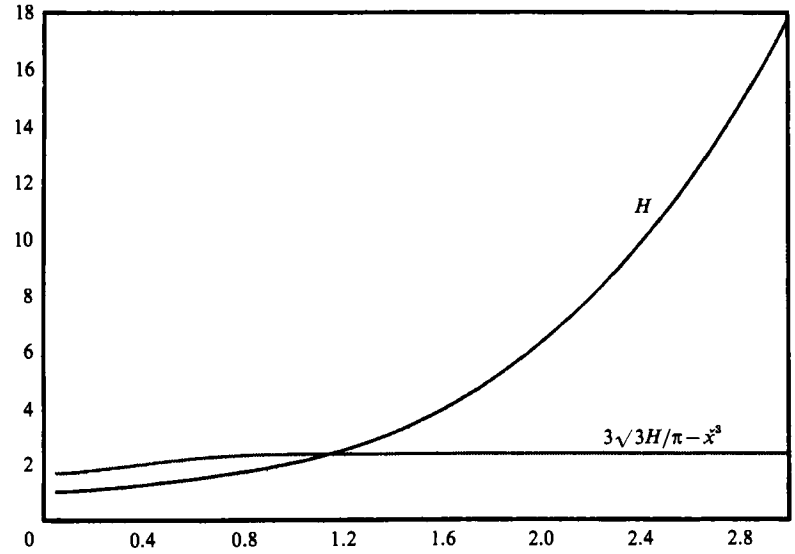

FIGURE 8. The numerical solution of the axisymmetric boundary-layer equations, (5.3) illustrating H and $3\sqrt{3H/\pi - \check{x}^3}$ which asymptotes to 2.33 as $\check{x} \to \infty$.

Here $x^* = 0$ corresponds to the point at which the jet hits the plate and Q is the flux falling onto the plate. We presume that at this point the flow is inviscid and so we find $h^* = \sigma^2/2x^*$, where σ is the radius of the jet as it strikes the plate and that a boundary layer grows from the wall to fill the layer downstream. We non-dimensionalize these equations, and introduce a stream function and modified vertical coordinate as follows:

$$x^* = L_\infty \check{x}, \quad L_\infty = \left(\frac{Q\sigma^2}{4\pi\nu}\right)^{\frac{1}{3}}, \tag{5.2a, b}$$

$$y^* = \frac{\sigma^2}{2L_\infty}\check{y}, \quad \check{z} = \check{y}\check{x}, \quad U^* = \frac{Q}{\pi\sigma^2}\check{\psi}_{\check{z}}. \tag{5.2c–e}$$

This leads to the equations

$$\check{U}\check{U}_{\check{x}} - \check{\psi}_{\check{x}}\check{U}_{\check{z}} = \check{x}^2\check{U}_{\check{z}\check{z}}, \tag{5.3a}$$

$$\check{U} = \check{\psi}_{\check{z}}, \tag{5.3b}$$

$$\check{U}(0) = \check{\psi}(0) = 0, \quad \check{U}_{\check{z}}(H) = 0, \quad \check{\psi}(H) = 1, \tag{5.3c}$$

$$\check{z} \in [0, H], \quad H \text{ unknown}, \tag{5.3d}$$

$$H = 1 \quad \text{at} \quad \check{x} = 0. \tag{5.3e}$$

These equations do not exhibit branching/free interaction since the interaction is suppressed by the neglect of the pressure term, $(sH/\check{x})_{\check{z}}$, due to the small value of s. Note that as H increases the interaction is reinstated.

The similarity solution to these equations, for large values of $\check{x}$, when viscous effects are assumed to be spread across the layer, is such that (see Watson 1964)

$$\check{\psi} = f(\xi), \quad \xi = \check{z}/H, \quad H = q(\check{x}^3 + d^3), \tag{5.4a}$$

$$f''' + 3qff'^2 = 0, \tag{5.4b}$$

$$f(0) = f'(0) = f''(1) = 0, \quad f(1) = 1, \tag{5.4c}$$

Q	σ	x_J^*	h_J^*
11	0.15	2.55	0.034
18	0.17	2.95	0.026
29	0.22	4.15	0.028

TABLE 1. The measurements of the experimental hydraulic jumps of Craik *et al.* (1981): the flux Q, the jet radius, σ, the jump position, x_J^*, and the depth just upstream of the jump, h_J^*

where the value of d^3 is to be found numerically by solving the initial value problem (5.3) and the prime represents $\partial/\partial\xi$. Then

$$q = \frac{\pi}{3\sqrt{3}}, \quad \check{\psi}_{\check{z}\check{z}}|_0 = \frac{3\sqrt{3}c^3}{2\pi}\frac{1}{H^2}, \quad \int_0^H \check{\psi}_{\check{z}}^2\,\mathrm{d}y = \frac{\sqrt{3}c}{\pi}\frac{1}{H}, \tag{5.4d–f}$$

where

$$c \approx 1.402. \tag{5.4g}$$

We integrate (5.3) forward in $\check{x}$ from an initial condition using a suitable adjustment of a Crank–Nicholson scheme. This initial condition consists of a uniform velocity for $\check{z} > 0$ and a velocity of zero for $\check{z} = 0$. The flow becomes fully developed with $H \sim (\pi/3\sqrt{3})(\check{x}^3 + d^3)$, as predicted by Watson's theory for $\check{x} \gg 1$. The value of d^3 is estimated to be 2.33, using 101 points in the vertical direction and an $\check{x}$-step of 0.001. This value is used later. It agrees well with Watson's approximate method which gives $d^3 = 2.29$, see figure 8.

We use the above theory and computations to give a value of, among other variables, h_J^*, the depth at the jump position, Re and s at the jump and L_J^*, the nominal lengthscale of the jump given by (2.12*c*) given x_J^*, Q^*, and σ. Values for these are read from figure 1 or, in the case of σ, estimated from the results presented in table 1 in Craik *et al.* The position of the jump is judged to be the crest of the obvious wave just upstream of the jump itself. The results are, using $\nu = 0.01$, $g = 981$, $\rho = 1.0$ and $T = 73$ in c.g.s. units,

$$L_\infty = 1.996(Q\sigma^2)^{\frac{1}{5}}, \tag{5.5a}$$

$$Q^* = \frac{Q}{2\pi x_J^*}, \quad \lambda = 2.279, \quad \int_0^1 \bar{\psi}_0'^2\,\mathrm{d}y = 0.773, \tag{5.5b–d}$$

$$h_J^* = 0.0380\frac{x_J^{*3} + 18.53Q\sigma^2}{Qx_J^*}, \quad Re = 15.91\frac{Q}{x_J^*}, \tag{5.5e,f}$$

$$s = 2.123\frac{(x_J^{*3} + 18.53Q\sigma^2)^3}{Q^5 x_J^*}, \quad \mu = 142\frac{x_J^*(x_J^{*3} + 18.53Q\sigma^2)}{Q^3}, \tag{5.5g,h}$$

$$\gamma = 0.0594\frac{Q^{33}x_J^{*9}}{(x_J^{*3} + 18.53Q\sigma^2)^{21}}(\mu - 1), \quad L^* = L_J^* = 2.476\frac{(x_J^{*3} + 18.53Q\sigma^2)^9}{Q^{14}x_J^{*4}}h_J^*. \tag{5.5i,j}$$

The values we take for σ, Q, and x_J^* are presented in table 1 together with a measured value for the depth of the layer at the jump. The non-dimensional values of the jump radius, x_J^*/L_∞, in the experiments are in the range 1.25–2.23 and are therefore above the value, of about $\check{x} = 1$, where these integrations indicate the flow has become fully developed. The values predicted for μ and γ are also of interest. For the jump with flux $Q = 11$ it turns out that $\mu \approx 5.76$ and $\gamma \approx 4.34 \times 10^9$, whilst for the case $Q = 29$ these values are 2.36 and 9.12×10^{10}. On these predictions therefore the

Q	x_J^*	h_J^*	s	L_∞	Re
11	2.55	0.029	0.049	1.25	68.67
18	2.95	0.025	0.017	1.61	97.13
29	4.15	0.031	0.023	2.23	111.2

TABLE 2. The predictions, using equations (5.5) for the inverse Froude number, s, and the Reynolds number of the jump, Re. L_∞ is the non-dimensional distance downstream of the jet at which the jump occurs

behaviour of the flow upstream of the jump will be dominated by capillary effects and the upstream influence will be wave-like. This is seen in figure 1. The lengthscale of the upstream influence for such large positive values of γ is given by (3.9) and is of order $6.8\times10^4\,L_J^*$ and $2.5\times10^5\,L_J^*$ respectively. This gives upstream-influence scales of $8.9h_J^* = 3.1$ mm and $5.6h_J^* = 1.6$ mm, which seem in good agreement with figure 1. The values of L_J^* are $1.3\times10^{-4}\,h_J^*$ and $3.4\times10^{-6}\,h_J^*$ in these cases. These scales are very short, obviously much shorter than the scales seen in the experiments. However, this scale is again appropriate to jumps governed solely by the pressure-displacement law $P = -A$. In the present jumps the dominant effect upstream is the capillary term γA_{XX} in $(2.11f)$ because of the large value of γ. The jump far downstream is caused by the gravitational pressure gradient, but as shown in §4 this only dominates at a distance $X \sim O(\gamma^{\frac{1}{2}})$ downstream. In unscaled, dimensional terms this translates as being a distance of the order of $8.7h_J^* = 3.0$ mm and $6.7h_J^* = 1.9$ mm in the cases $Q = 11$ and $Q = 29$ respectively. It is encouraging to find that this length is of the order of that seen in the experimental results. The predictions for the Reynolds number, inverse Froude number and layer depth at the jump position, as well as the non-dimensional radius of the jump are presented in table 2. It can be seen that the prediction for the layer depth at the jump position is extremely good.

5.2. *The prediction for the jump height*

Using this theory to give the flow upstream of the jump, we may now go ahead and use the results of §§3 and 5.1 together with those of Gajjar & Smith (1983) to predict the free-surface shape, $h^*(x)$, downstream. It can be shown that the profile far downstream of the jump position, on the lengthscale L_J^* has

$$\frac{\delta h^*}{h_J^*} = 0.947\,96\frac{s}{\lambda^2}\left(\frac{\lambda^5(\delta x^*)}{Re\,s^3 h_J}\right)^{0.4305}, \tag{5.6}$$

where δx^* denotes the distance downstream and δh^* the change in height. This assumes that the jump occurs on a lengthscale short compared with its radius, allowing us to neglect its axisymmetric form and approximate it as two-dimensional.

We can either use the predictions of Watson's theory, (5.5), to give values for h_J^* given x_J^* or, alternatively, we can measure h_J^* from figure 1. The first approach gives the prediction

$$\frac{\delta h^*}{h_J^*} = 1.071\frac{Q^{1.4574}x_J^{*1.1525}}{(x_J^{*3}+18.53Q\sigma^2)^{1.305}}(\delta x^*)^{0.4305}, \tag{5.7}$$

whilst the second leads to

$$\delta h^* = 0.0150\frac{Q^{0.1525}}{h_J^{*0.305}x_J^{*0.1525}}(\delta x^*)^{0.4305}. \tag{5.8}$$

Q	δh^*			$\delta h^*/h_J^*$		
δx^*...	0.25	0.5	1.0	0.25	0.5	1.0
11	0.0375	0.0625	0.1	1.103	1.84	2.94
18	0.0375	0.075	0.119	1.44	2.88	4.56
29	0.0313	0.0625	0.103	1.12	2.23	3.68

TABLE 3. The measurements of the jump – the increase in depth δh^* and the relative increase $\delta h^*/h_J^*$ at positions 0.25, 0.5 and 1.0 cm downstream

Q	$\delta h^*/\delta m^{*m}$	$\delta h^*\|_{\delta x^*=0.25}$	$\delta h^*\|_{\delta x^*=0.5}$	$\delta h^*\|_{\delta x^*=1.0}$
11	0.058	0.031 (81%)	0.041 (66%)	0.055 (55%)
18	0.063	0.033 (89%)	0.045 (60%)	0.061 (51%)
29	0.062	0.032 (103%)	0.043 (69%)	0.058 (56%)

TABLE 4. A comparison of the measurements of table 2 with the predictions of (5.7) for the absolute increase in the depth. The percentage figures give the ratio of the predicted to the measured result

Q	$\delta h^*/h_J^* \delta x^{*m}$	$\delta h^*/h_J^*\|_{\delta x^*=0.25}$	$\delta h^*/h_J^*\|_{\delta x^*=0.5}$	$\delta h^*/h_J^*\|_{\delta x^*=1.0}$
11	1.93	1.06 (99%)	1.43 (80%)	1.93 (68%)
18	2.40	1.32 (92%)	1.78 (62%)	2.40 (52%)
29	1.90	1.04 (93%)	1.41 (63%)	1.90 (52%)

TABLE 5. A comparison of the measurements of table 2 with the predictions of (5.7) for the relative increase in the depth. The percentage figures give the ratio of the predicted to the measured result

We choose to measure δx^* and δh^* from the final dip in the jump profile, just upstream of the jump proper. This is not from the x^*-station we use to non-dimensionalize the equations. The predictions above are valid far downstream where capillary effects are small, but the change in height from h_J^* is δh^* plus a constant due to the effects of surface tension. We attempt to model the effects of this constant by the above choices for δx^* and δh^*. However, given the experimentally very large values of γ and so the large downstream shift in x^* before the effects of gravity become important and the above predictions can be taken to be valid, this arbitrary choice cannot be expected to be accurate (see below). The measurements of δh^* for $\delta x^* = 0.25$, 0.5 and 1.0 cm, taken from figure 1 are presented in table 3.

The predictions of (5.7) are given in tables 4 and 5, together with the ratio of the predicted to the measured result written in percentage terms. These results are also presented in graphical format in figure 9. The prediction is most accurate for smaller values of δx^*, where it is quite good. Similar behaviour is seen in the predictions of (5.8) in tables 6 and 7 A second possibility in making the comparison is to compare these predicted curves with the shape of the jump as it nears its maximum depth on the assumption that the large value of γ delays the position of applicability of the predictions to this point. Although the positioning of the curves is arbitrary the agreement in figure 9 can be excellent. Further downstream we cannot expect the prediction to be valid since then the value of $-A$ has become so large that the linearization (within the outer region) implicit in deriving (2.10) is no longer valid. Viscous effects also grow to be important in Region I of figure 3 as δx^* increases, and

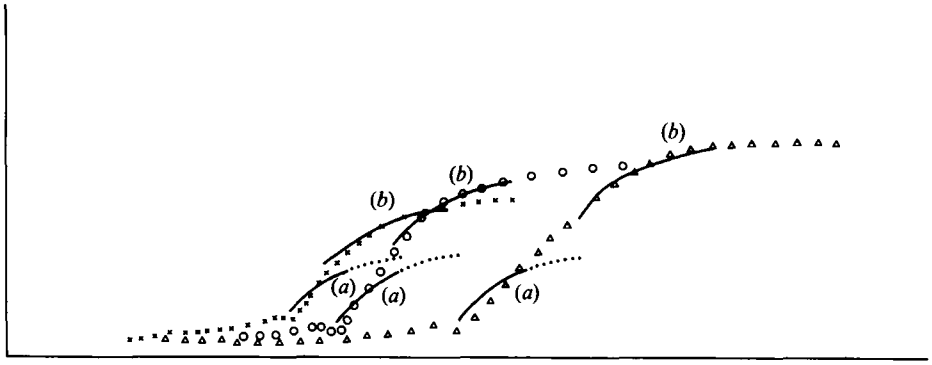

FIGURE 9. Comparisons between experiments (×, ○, △ representing the $Q = 11$, 18, 29 experiments of Craik *et al.*) and the present theory (——, and marked (*a*), from (5.7)), for the free-surface shape, in three different cases. The dotted curves indicate the continuations of (5.7) which, however, apply only for a restricted range of distances x^*: see the text. The curves marked (*b*) are the result of shifting those marked (*a*) in x^* and depth by an arbitrary amount in order to model the effect of surface tension on this downstream prediction — see §4.

Q	$\delta h^*\|_{\delta x^*=0.25}$	$\delta h^*\|_{\delta x^*=0.5}$	$\delta h^*\|_{\delta x^*=1.0}$
11	0.029 (77%)	0.039 (62%)	0.053 (52%)
18	0.033 (88%)	0.044 (60%)	0.060 (51%)
29	0.033 (106%)	0.044 (71%)	0.060 (58%)

TABLE 6. A comparison of the measurements of table 2 with the predictions of (5.8) for the absolute increase in the depth. The percentage figures give the ratio of the predicted to the measured result

Q	$\delta h^*/h_J^*\|_{\delta x^*=0.25}$	$\delta h^*/h_J^*\|_{\delta x^*=0.5}$	$\delta h^*/h_J^*\|_{\delta x^*=1.0}$
11	0.82 (77%)	1.10 (62%)	149 (52%)
18	1.27 (88%)	1.72 (60%)	2.31 (51%)
29	1.10 (106%)	1.59 (71%)	2.14 (58%)

TABLE 7. A comparison of the measurements of table 2 with the predictions of (5.8) for the relative increase in the depth. The percentage figures give the ratio of the predicted to the measured result

the axisymmetric nature of the flow, while negligible during the local jump process, becomes a significant additional influence downstream.

6. Concluding comments

The comparison presented above seems supportive of the present proposal that these hydraulic jumps are governed by a free interaction predominantly between surface tension and viscosity upstream and then further downstream between the gravitational pressure gradient and viscosity. Viscous effects, then, are vital in controlling these jumps. Downstream conditions play a role in determining the position of the jumps.

The theory reproduces much of the structure seen in the experiments, as well as the general jump profile. For example, the shortening of the lengthscale of the jump, for a given flux Q, as the jump nears the source of the axisymmetric liquid layer and the

Froude number of the flow is increased is predicted by equation (5.5). The capillary effects on the upstream side of the jump are reproduced, the predicted upstream scales being of the order of a few multiples of the layer's depth. Experiments with liquids of different surface-tension coefficients would be of interest in testing the importance of the value of μ (equation (2.12*b*)) since it is this that determines whether or not waves are predicted upstream of the jump. A change from wave-like behaviour to smooth upstream influence is to be expected as μ becomes less than one and the effects of streamline curvature dominate over those of surface tension. This change is seen in the results of §3 for flow over a small obstacle and in the computations of the free interaction in §4 (see figure 7). In addition we can expect there to be a noticeable effect on the scales of the jump and upstream influence as γ is reduced in magnitude when $\mu \approx 1$. It is helpful that the experiments are relatively simple to perform, the hydraulic jumps being a commonly seen phenomenon, providing a useful check on the predictions of this particular application of interactive-flow theory. Predictions similar to these are made by Bowles (1990) in a discussion of the changes of shape of hydraulic jumps to be expected on a slope as the slope angle increases. We note in addition that there may well be applications of this theory, and in particular its predictions for the relatively sudden swelling of the layer thickness, in the areas of ground effects for vertical-take-off vehicles and other situations involving hot or cold thin layers or wall jets (Professors P. Blythe, P. G. Daniels, J. Scott and Dr K. Winters, private communications 1989–90. Also S. J. Parkinson's unpublished Ph.D. thesis work 1986–88). In general the pressure-displacement law for these physical situations is $P = \pm A \pm A_{XX}$ and some computational results have been obtained for these cases. The parameter regime of the experiments corresponds to large values of γ and it would be of interest, also, if the short eddies discussed in §4 are seen experimentally. Indeed there is a case for taking the study of the large-γ limit further since increasing γ increases the lengthscale of the free interaction opposing the effect of the large values of the Froude number and so returning the lengthscale towards the $O(Re)$ values (see §2).

On the downstream side of the jump gravity is important despite the extremely large value of γ. The distance downstream at which the blunt shape emerges is in line with the predicted value of a few layer depths. The solutions for the free interactions for the case $\gamma > 0$ suggest that once the boundary layer has finally separated there are no further oscillations in depth and the increase becomes monotonic, eventually giving rise to a blunt shape as the effects of surface tension become less important. The predictions for the lengths over which this occurs, and so the length of the jump, can only be taken as approximate due to the very strong dependence of L_J^* and γ on x_J^*, see (5.5*i*) and (5.5*j*). If $x_J^* \gg 18.53Q\sigma^2$ then $L_J^* \sim x_J^{*23}$ and $\gamma \sim x_J^{*-54}$ and this makes the predictions very susceptible to errors made in measuring x_J^* from figure 1. The predictions (and the position of the curves (*b*) in figure 9), are also very dependent on the accuracy with which Q is measured. Indeed all the results are liable to this type of error, for example an error of 5% in x_J^* leads to an 11% error in the predictions for $\delta h^*/h_J^*$ presented in table 5. The predictions are still reasonably accurate, however, especially near the start of the jump.

As a final comment it is worth noting that the high-Reynolds-number theory seems to be successful in describing the part of the jump where the flow separates, despite the relatively small value of Re in the experiment (approximately 100). A full description of the jump requires the study of the flow downstream of this point and the subsequent development and reattachment of the flow. This may enable the influence of the downstream boundary condition to be determined explicitly. The

models of the flow of a separated free shear layer over an eddy developed by Peregrine (1974) and Teles da Silva & Peregrine (1975) may be of some relevance here for the case $\gamma < 0$. In the general case, it seems that the fluid moving over the separated region can develop, on the long lengthscale of the separation bubble, into a sech^2-jet profile, free from the effects of contact with the wall and subject to an adverse pressure gradient, decreasing in magnitude. On the other hand, in the experimental jump the effects of axisymmetry will now be free to thin the layer, causing a favourable pressure gradient and reattachment. This is clearly a complicated process.

The comments of the referees are gratefully acknowledged as is the financial support of SERC for R.I.B.

REFERENCES

BENJAMIN, T. B. 1962 The solitary wave on a stream with an arbitrary distribution of vorticity. *J. Fluid Mech.* **12**, 97–112.

BOWLES, R. I. 1990 Applications of nonlinear viscous-inviscid interactions in liquid layer flows & transonic boundary layer transition. Ph.D. thesis, University of London.

BROTHERTON-RATCLIFFE, R. V. & SMITH, F. T. 1986 Boundary layer effects in liquid layer flows. Ph.D. thesis, chapter 3, University of London.

BROWN, S. N., STEWARTSON, K. & WILLIAMS, P. G. 1975 On expansive free interactions in boundary layers. *Proc. R. Soc. Edinb.* **74**A, 21.

CLARKE, W. O. 1970 Tap-splash and the hydraulic jump. *School Sci. Rev.* **152**, 67.

CRAIK, A. D. D., LATHAM, R. C., FAWKES, M. J. & GRIBBON, P. W. F. 1981 The circular hydraulic jump. *J. Fluid Mech.* **112**, 347.

GAJJAR, J. S. B. & SMITH, F. T. 1983 On hypersonic self-induced separation, hydraulic jumps and boundary layers with algebraic growth. *Mathematika* **30**, 77.

LAMB, H. 1932 *Hydrodynamics.* Cambridge University Press.

LARRAS, M. J. 1962 Ressaut circulaire sur fond parfaitement lisse. *C. R. Acad. Sci. Paris* **225**, 837.

LIGHTHILL, M. J. 1978 *Waves in Fluids.* Cambridge University Press.

PEREGRINE, D. H. 1974 Surface shear waves. *J. Hydraul. Div.*, ASCE **100**, 1215.

RAYLEIGH, LORD 1914 *Proc. R. Lond. Soc.* A **90**, 324 and *Scientific Papers*, vol. 6, p. 250. Cambridge University Press.

SMITH, F. T. 1976*a* Flow through constricted or dilated pipes and channels: Part 1. *Q. J. Mech. Appl. Maths* **29**, 343.

SMITH, F. T. 1976*b* Flow through constricted or dilated pipes and channels: Part 2. *Q. J. Mech. Appl. Maths* **29**, 365.

SMITH, F. T. 1977 Upstream interactions in channel flow. *J. Fluid Mech.* **79**, 631.

SMITH, F. T. 1978 Flow through symmetrically constricted tubes. *J. Inst. Maths Applics.* **21**, 145.

SMITH, F. T. 1982 On the high Reynolds number theory of laminar flows *I.M.A. J. Appl. Maths* **28**, 207.

SMITH, F. T. 1985 On large-scale eddy closure. *J. Math. Phys. Sci.* **19**, 1–80.

SMITH, F. T. 1988 Finite-time break-up can occur in any unsteady interactive boundary layer. *Mathematika* **35**, 256.

SMITH, F. T. & DUCK, P. W. 1977 Separation of jets and thermal boundary layers from a wall. *Q. J. Mech. Appl. Maths* **30**, 143.

TELES DA SILVA, A. F. & PEREGRINE, D. H. 1988 Steep, steady surface waves on water of finite depth with constant vorticity. *J. Fluid Mech.* **195**, 281.

WATSON, E. J. 1964 The radial spread of a liquid jet over a horizontal plane. *J. Fluid Mech.* **20**, 481.